JOM, Vol. 68, No. 10, 2016
DOI: 10.1007/s11837-016-2064-1

Hard Carbon Fibers Pyrolyzed from Wool as High-Performance Anode for Sodium-Ion Batteries

XIAOMING ZHU,[1] QIAN LI,[2] SHEN QIU,[3] XIAOLING LIU,[1] LIFEN XIAO,[4] XINPING AI,[3] HANXI YANG,[3] and YULIANG CAO[3,5]

1.—Hubei Collaboration Innovation Center of Non-power Nuclear Technology, School of Nuclear Technology & Chemistry and Biology, Hubei University of Science and Technology, Xianning 437100, China. 2.—College of Chemistry and Chemical Engineering, Wuhan Textile University, Wuhan 430073, China. 3.—Hubei Key Lab. of Electrochemical Power Sources, College of Chemistry and Molecular Science, Wuhan University, Wuhan 430072, China. 4.—College of Chemistry, Central China Normal University, Wuhan 430079, China. 5.—e-mail: ylcao@whu.edu.cn

In this paper, we first demonstrate that the wool from worn-out clothes can serve as a low-cost and easy-to-collect precursor to preparing high-performance hard carbons for Na-ion batteries. Morphological characterizations demonstrate that this wool-derived hard carbon presents well-defined and homogeneously dispersed fiber networks. X-ray diffraction results combined with high-resolution transmission electron microscopy analysis reveal that the interlayer space (d(002)) of the graphitic layers is 0.376 nm, sufficient for Na insertion into the stacked graphene layers. Electrochemical results show that the wool-derived hard carbon can deliver a high capacity of 303 mAh g^{-1} and excellent cycle stability over 80 cycles. This satisfactory electrochemical performance and easy synthetic procedure make it a promising anode material for practical SIBs.

INTRODUCTION

The global energy crisis and environmental pollution have spurred intensive research on large-scale energy storage (EES) technologies so as to integrate renewable energy sources such as solar and wind into electric grids. Recently, room-temperature sodium-ion batteries (SIBs) have attracted much interest as a promising alternative to lithium-ion batteries (LIBs) for EES applications due to sodium's natural abundance, low cost and environmental friendliness.[1–8]

To achieve affordable Na-ion technologies, it is of great importance to develop high-performance and low-cost Na-storage electrodes, especially anode materials.[9–15] Up to now, various host frameworks such as metal oxides,[16–18] alloys[19–21] and phosphorous[22–24] have been proposed for anode applications, among which carbonaceous materials have received particular attention due to their low operation potential (0–1.0 V), high capacity (250–430 mAh g^{-1}) and easy preparation.[25–31] Nevertheless, it still remains a great challenge to develop superior Na-storage carbonaceous materials because of the much larger radius of Na ions (0.102 nm) compared with Li ions (0.076 nm). Graphite materials, the most widely used anode materials in Li-ion batteries, exhibit very poor electrochemical performance in conventional Na-ion batteries, possibly due to their limited graphitic interlayer distance (0.34 nm).[32,33] In this condition, disordered hard carbons with a larger interlayer spacing (0.36–0.43 nm) and abundant nanovoids appear to be a feasible approach for Na-storage anode materials. Dahn first reported reversible Na insertion behavior into glucose-pyrolyzed hard carbons, with a high capacity of 300 mAh g^{-1} and a low insertion potential of <0.2 V (versus Na^+/Na).[34] Subsequently, a variety of hard carbons designed with unique morphologies or hierarchically porous structures demonstrated superior Na-storage performance, such as carbon hollow nanowires, hollow nanospheres, nanofibers, nanosheets, and so on. The precursors of hard carbons are mainly artificial polymers (polyailine,[28] polyacrylonitrile,[35] furfural resin,[36] etc.) and natural biomass wastes (peat moss,[37] banana peel,[38] pomelo peel,[39] apple peel,[40]

Xiaoming Zhu and Qian Li have contributed equally to this work.

(Published online August 8, 2016)

etc.), the latter offering the better choice for preparing hard carbons on the basis of cost and recyclability. Furthermore, these hard carbons can to some extent inherit the unique morphology, structure and properties of the natural biomass. For instance, Mitlin synthesized carbon nanosheet frameworks by utilizing peat moss as the raw material, and discovered that they could deliver a reversible capacity of 298 mAh g^{-1} and superior rate performance.[37] The hard carbon nanofibers derived from bleached pulp showed a specific capacity of 255 mAh g^{-1} and excellent cycle stability of 600 cycles. Very recently, Xu introduced pomelo peel as the precursor to synthesize hard carbons, which were able to realize a very high capacity of 430 mAh g^{-1} and ~98% capacity retention over 200 cycles.[39] Therefore, it is of great importance to develop low-cost and easy-to-collect precursors for the fabrication of high-performance hard carbons.

As the most important raw material in the textile industry, wool has been widely used in clothing, carpets, etc. However, worn-out wool products have little economic value and are abandoned directly as biodegradable wastes. Here, we demonstrate that worn-out wool can serve as an ideal precursor for the preparation of high-performance hard carbons, with a high capacity of 303 mAh g^{-1} and good capacity retention of 92% over 80 cycles.

EXPERIMENTAL DETAILS

Material Synthesis and Characterizations

The wool was put into a tube furnace and carbonized at 1100°C for 2 h under Ar flow with a ramping rate of 2°C/min to prepare the hard carbon fibers.

The morphological features of the wool-derived hard carbon fibers were characterized by scanning electron microscopy (SEM; Ultra/Plus, Zeiss) and by transmission electron microscopy (TEM; JEOL, JEM-2010-FEF). The crystalline structures of carbon were characterized by x-ray diffraction (XRD; Shimadzu XRD-6000). Raman spectra were obtained using a Digilab FTS3500 (Bio-Rad) with a laser wavelength of 532 nm. The surface area and porous structure were analyzed by nitrogen adsorption–desorption measurements (ASAP 2020; Micromeritics, USA). The surface area was derived from the adsorption isotherm based on the Brunauer–Emmett–Teller (BET) equation, and the porous volume and average pore size were determined by the Barrett–Joyner–Halenda model.

Electrochemical Measurements

The wool-derived carbon fiber anode was prepared by mixing 80 wt.% hard carbon fibers, 10 wt.% super P and 10 wt.% polyacrylic acid to form a slurry, which was then coated onto a copper (Cu) foil and dried at 60°C overnight under vacuum. The charge–discharge performances of the electrode were examined by 2016 coin-type cells using the

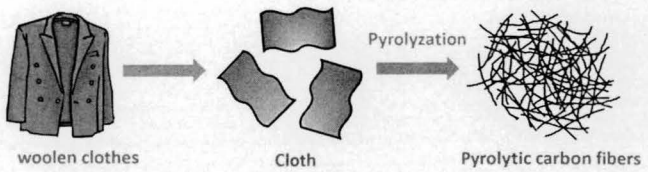

Fig. 1. Synthesis scheme of wool-derived hard carbon.

woolen carbon fiber anode as a working electrode and a Na sheet as the counter and reference electrode, 1 M $NaClO_4$ in ethylene carbonate (EC) diethylcarbonate (DEC) (1:1 by volume) with 5% fluoroethylene carbonate (FEC) as the electrolyte, and a Celgard 2400 microporous membrane as the separator. The Na sheets were home-made by rolling sodium lumps onto a plate, and then cut into circulated disks. All the cells were assembled in a glove-box with the water/oxygen content lower than 1 ppm and tested at room temperature. The galvanostatic charge–discharge test was conducted on a LAND cycler (Wuhan Kingnuo Electronic, China). Cyclic voltammetric measurements were carried out with the coin cells at a scan rate of 0.1 mV s^{-1} using a CHI 660c electrochemical work station (ChenHua Instruments, China).

RESULTS AND DISCUSSION

The main composition of wool is keratin, which exhibits a long spiral macromolecular chain structure. The highly cross-linked structure can form nongraphitic carbon at a reasonable pyrolysis temperature, which permits the use of Na ions. Figure 1 illustrates the one-step synthetic procedure of hard carbons from worn-out wool clothing. As can be seen, the recycled clothes are first cut into small pieces, and then pyrolyzed at 1100°C for 2 h under an inert atmosphere. Due to its pristine interconnected networks of woolen textile fabric, the as-prepared hard carbons can be expected to possess similar fibrous structures with long fibers interconnecting with others to build a conductive network, facilitating fast electron transportation.

Morphological features of the as-prepared hard carbons were characterized by SEM measurement. As shown in Fig. 2a and b, the wool-derived hard carbons mainly appear as fiber networks interconnected by randomly aligned and uniformly dispersed carbon fibers, which may favor electronic and ionic transportation. Each fiber is long and straight, and has a uniform diameter of 4–5 μm. It can be seen from Fig. 2b that the surface of a single fiber is partly rough, and resembles the joint structure of bamboo. The rough surface possibly results from the gas evolution during pyrolysis, which can effectively increase the contact between the electrode and the electrolyte. The high-resolution transmission electron microscopy (HRTEM) image shown in Fig. 2c reveals the weakly ordered turbostratic structure of this hard carbon, having a short-range aligned lattice. The carbon layer

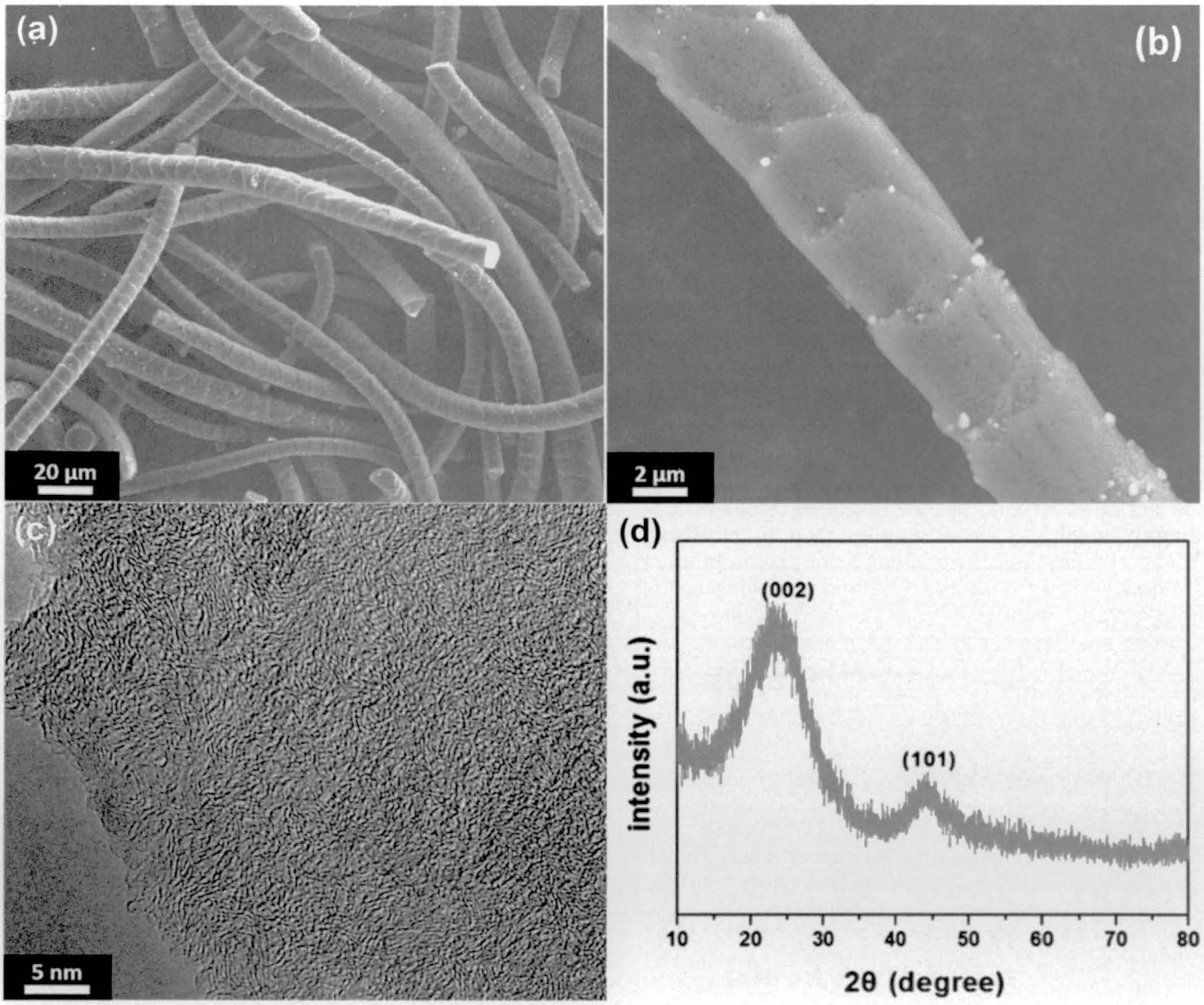

Fig. 2. (a, b) SEM image; (c) HRTEM image; (d) XRD pattern of wool-derived hard carbon.

spacing can be measured as ~0.37 nm, larger than that of graphite. The XRD patterns of the hard carbon are given in Fig. 2d. Two characteristic diffraction peaks appear at ~23.0° and ~43.6°, and can be indexed to the (002) and (100) planes of graphitic microcrystalline. The weak and broad diffraction peaks indicate the disordered state of this carbon, consistent with the HRTEM observation in Fig. 2c. According to Bragg's formula, the average interlayer spacing (d_{002}) value of the carbon can be calculated to be ~0.376 nm, which is larger than that (0.335 nm) of the graphite. Cao et al. used theoretical simulations on the energy cost for Na-ion insertion into carbon as a function of the carbon interlayer distance and found the energy barrier to be low enough to permit the insertion and extraction of Na ions when the d-space increases to about 0.37 nm.[28] Thus, the large interlayer spacing of the as-prepared hard carbon should prove to be appropriate for Na-ion insertions into the carbon layers.

The crystalline structure of the wool-derived hard carbon has been further characterized by Raman spectroscopy analysis. As shown in Fig. 3a, two main Raman peaks can be observed at 1590 cm^{-1} and 1355 cm^{-1}, corresponding to the vibration mode of the graphitic layers (G band) and disordered graphitic structures (D band), respectively. In general, the integral intensity ratio of these two peaks (I_D/I_G) decreases with the degree of graphitic ordering in the carbons. The large intensity ratio of the D band to the G band (I_D/I_G = 1.85) is in good agreement with that of commercial hard carbon pyrolyzed at 1100°C,[37–40] exhibiting a disorder structured to some extent. The porous structures of the carbon

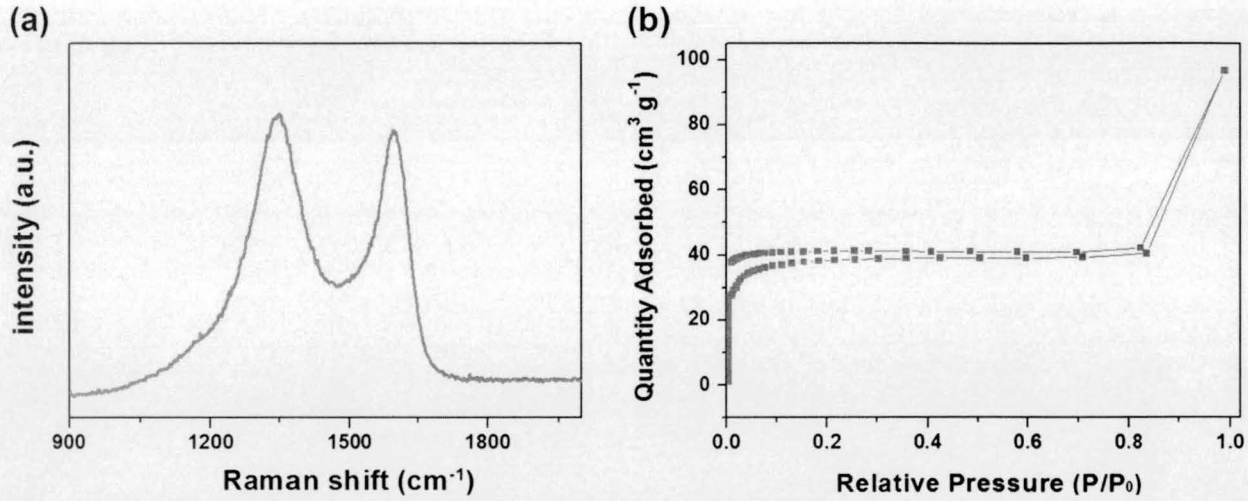

Fig. 3. (a) N_2 adsorption–desorption; (b) pore size distribution curve of wool-derived hard carbon.

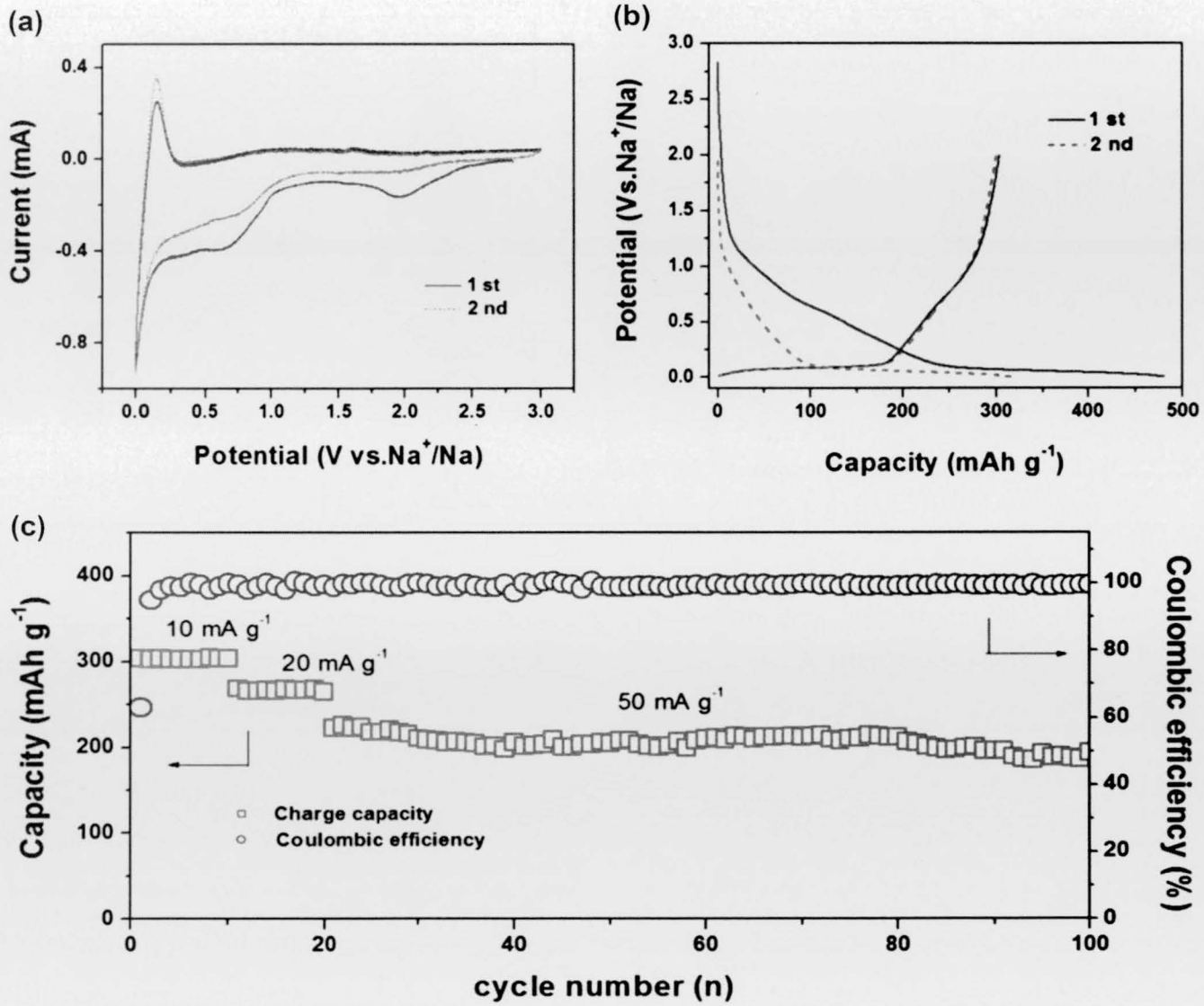

Fig. 4. Electrochemical characterization of the wool-derived hard carbon electrode. (a) Cyclic voltammograms at a scan speed of 0.1 mV s^{-1} at 0–3.0 V; (b) the charge–discharge curves at a current density of 10 mA g^{-1}; (c) cycling performance.

fibers have been investigated by N_2 adsorption–desorption measurements in Fig. 3b. The specific BET surface area was 152 $m^2\ g^{-1}$. The large surface area could provide a large electrochemical reaction area to improve Na^+ storage properties. The pore volume and average pore size were 0.15 $cm^3\ g^{-1}$ and 3.9 nm, respectively.

The electrochemical Na-storage performance of the wool-derived hard carbon electrode has been investigated by cyclic voltammetric (CV) and galvanostatic charge–discharge tests. Figure 4a shows the first two CV scans at a scan rate of 0.1 mV s^{-1}. As can be seen, the main CV features appear as a pair of sharp and symmetrical oxidation/reduction peaks at ~0.15/0.01 V, respectively. According to most literature,[35,36] this pair of oxidation/reduction peaks correspond to the Na-ion extraction/insertion reactions into the graphene layers. In addition, two broad cathodic peaks at ~2.0 V and ~0.75 V could be observed during the first scan, attributed to the decomposition of the electrolyte and the formation of a SEI layer on the carbon surface.

Figure 4b shows the charge–discharge profiles of the hard carbon electrode measured between 0 and 2.0 V at a current rate of 10 mA g^{-1}. In accordance with the CV curves, the electrode demonstrates two distinguishable reaction potential areas at 2–0.1 V and 0.1–0 V, which can be attributed to the adsorption on the active sites of the surface and the insertion into the carbon layers of Na ions, respectively. The charge and discharge capacity in the first cycle were 303 mAh g^{-1} and 480 mAh g^{-1}, respectively, corresponding to an initial coulombic efficiency of 63%. But, in the second cycle, the charge profile stayed nearly unchanged, and the coulombic efficiency increased up to ~99.5%, indicating a good reversibility of the Na insertion reactions. Compared to biomass-derived hard carbon, for example, apple peel, bleached pulp, lignin, etc.,[40–42] this wool-derived hard carbon exhibits a higher Na-storage capacity, possibly originating from its suitable layer spacing and interconnected fiber-like framework. More importantly, the charge capacity below 1.0 V comprises ~80% of its whole Na-storage capacity, offering great benefits to enhance the energy density of Na-ion full cells.

The rate and cycling performance of this hard carbon electrode is displayed in Fig. 4c. As shown, the reversible capacity of the electrode is 303 mAh g^{-1}, 265 mAh g^{-1} and 222 mAh g^{-1} at current densities of 10 mAh g^{-1}, 20 mAh g^{-1} and 50 mA g^{-1}, respectively, with a coulombic efficiency of ~99.5% during cycling. When this electrode cycled at a current density of 50 mA g^{-1}, the specific capacity faded slightly from 210 mAh g^{-1} to 190 mAh g^{-1}, corresponding to excellent capacity retention of 92% over 80 cycles. The good rate performance and satisfactory cycle stability of the wool-derived hard carbon is probably due to its unique structure, with fibers interconnected with each other to enhance the electronic conductivity and buffer the volumetric change during Na ion insertion and extraction.

CONCLUSION

In summary, abandoned wool textiles as precursors have been used to prepare hard carbon fibers. The as-prepared hard carbons inherit the fibrous interconnected frameworks of the wool with a uniform diameter of 4–5 μm and a carbon layer spacing of ~0.37 nm. The electrochemical tests demonstrated good Na-storage performance with a high reversible capacity of 303 mAh g^{-1} and an impressive capacity retention of 92% over 80 cycles, offering a potential application possibility for Na-ion batteries for large-scale energy storage. Additionally, the preparation of the hard carbon from the worn-out clothes as anode material is a good idea, which not only increases the economic value but also avoids environmental waste.

ACKNOWLEDGEMENT

The authors gratefully acknowledge the financial support by the 2011 Program of Hubei Province, Natural Science Foundation of Hubei Province, China (Grant No. 2015CFC774), Program for New Century Excellent Talents in University (NCET-12-0419) and Hubei National Funds for Distinguished Young Scholars (2014CFA038).

REFERENCES

1. B.L. Ellis and L.F. Nazar, *Curr. Opin. Solid State and Mater. Sci* 16, 168 (2012).
2. S.-W. Kim, D.-H. Seo, X. Ma, G. Ceder, and K. Kang, *Adv. Energy Mater.* 2, 710 (2012).
3. M.D. Slater, D. Kim, E. Lee, and C.S. Johnson, *Adv. Funct. Mater.* 23, 947 (2013).
4. H. Li, C. Wu, F. Wu, and Y. Bai, *Acta Chim. Sin.* 72, 21 (2014).
5. K.B. Hueso, M. Armand, and T. Rojo, *Energy Environ. Sci.* 6, 734 (2013).
6. V. Palomares, M. Casas-Cabanas, E. Castillo-Martinez, M.H. Han, and T. Rojo, *Energy Environ. Sci.* 6, 2312 (2013).
7. V. Palomares, P. Serras, I. Villaluenga, K.B. Hueso, J. Carretero-Gonzalez, and T. Rojo, *Energy Environ. Sci.* 5, 5884 (2012).
8. H. Pan, Y.-S. Hu, and L. Chen, *Energy Environ. Sci.* 6, 2338 (2013).
9. M. Dahbi, N. Yabuuchi, K. Kubota, K. Tokiwa, and S. Komaba, *Phys. Chem. Chem. Phys.* 16, 15007 (2014).
10. H.N. He, H.Y. Wang, Y.G. Tang, and Y.N. Liu, *Prog. Chem.* 26, 572 (2014).
11. Y. Kim, K.H. Ha, S.M. Oh, and K.T. Lee, *Chem. Eur. J.* 20, 11980 (2014).
12. X.G. Han, Y. Liu, Z. Jia, Y.C. Chen, J.Y. Wan, N. Weadock, K.J. Gaskell, T. Li, and L.B. Hu, *Nano Lett.* 14, 139 (2014).
13. N. Yabuuchi and S. Komaba, *Sci. Technol. Adv. Mater.* 15, 1468 (2014).
14. L. Xiao, Y. Cao, W.A. Henderson, M.L. Sushko, Y. Shao, J. Xiao, W. Wang, M.H. Engelhard, Z. Nie, and J. Liu, *Nano Energy* 19, 279 (2016).
15. L. Wu, H. Lu, L. Xiao, X. Ai, H. Yang, and Y. Cao, *J. Mater. Chem. A* 3, 5708 (2015).
16. Y. Ansari, B. Guo, J.H. Cho, K. Park, J. Song, C.J. Ellison, and J.B. Goodenough, *J. Electrochem. Soc.* 161, A1655 (2014).

17. Z. Bi, M.P. Paranthaman, P.A. Menchhofer, R.R. Dehoff, C.A. Bridges, M. Chi, B. Guo, X.-G. Sun, and S. Dai, *J. Power Sources* 222, 461 (2013).
18. L.M. Wu, D. Buchholz, D. Bresser, L.G. Chagas, and S. Passerini, *J. Power Sources* 251, 379 (2014).
19. S. Qiu, X. Wu, L. Xiao, X. Ai, H. Yang, and Y. Cao, *ACS Appl Mater. Interfaces* 8, 1337 (2016).
20. L. Wu, X.H. Hu, J.F. Qian, F. Pei, F.Y. Wu, R.J. Mao, X.P. Ai, H.X. Yang, and Y.L. Cao, *Energy Environ. Sci.* 7, 323 (2014).
21. L. Xiao, Y. Cao, J. Xiao, W. Wang, L. Kovarik, Z. Nie, and J. Liu, *Chem. Commun.* 48, 3321 (2012).
22. J. Qian, X. Wu, Y. Cao, X. Ai, and H. Yang, *Angew. Chem. Int. Ed.* 52, 4633 (2013).
23. Y. Kim, Y. Park, A. Choi, N.S. Choi, J. Kim, J. Lee, J.H. Ryu, S.M. Oh, and K.T. Lee, *Adv. Mater.* 25, 3045 (2013).
24. J. Song, Z. Yu, M.L. Gordin, S. Hu, R. Yi, D. Tang, T. Walter, M. Regula, D. Choi, and X. Li, *Nano Lett.* 14, 6329 (2014).
25. C. Bommier, W. Luo, W.Y. Gao, A. Greaney, S.Q. Ma, and X. Ji, *Carbon* 76, 165 (2014).
26. V.G. Pol, E. Lee, D.H. Zhou, F. Dogan, J.M. Calderon-Moreno, and C.S. Johnson, *Electrochim. Acta* 127, 61 (2014).
27. X.-F. Luo, C.-H. Yang, Y.-Y. Peng, N.-W. Pu, M.-D. Ger, C.-T. Hsieh, and J.-K. Chang, *J. Mater. Chem. A* 3, 10320 (2015).
28. Y. Cao, L. Xiao, M.L. Sushko, W. Wang, B. Schwenzer, J. Xiao, Z. Nie, L.V. Saraf, Z. Yang, and J. Liu, *Nano Lett.* 12, 3783 (2012).
29. Y. Wen, K. He, Y.J. Zhu, F.D. Han, Y.H. Xu, I. Matsuda, Y. Ishii, J. Cumings, and C.S. Wang, *Nat. Commun.* 5, 4033 (2014).
30. J. Zhao, L.W. Zhao, K. Chihara, S. Okada, J. Yamaki, S. Matsumoto, S. Kuze, and K. Nakane, *J. Power Sources* 244, 752 (2013).
31. J. Jin, Z.Q. Shi, and C.Y. Wang, *Electrochim. Acta* 141, 302 (2014).
32. S.Y. Hong, Y. Kim, Y. Park, A. Choi, N.-S. Choi, and K.T. Lee, *Energy Environ. Sci.* 6, 2067 (2013).
33. S.L. Chou, Y.D. Pan, J.Z. Wang, H.K. Liu, and S.X. Dou, *Phys. Chem. Chem. Phys.* 16, 20347 (2014).
34. D. Stevens and J. Dahn, *J. Electrochem. Soc.* 147, 1271 (2000).
35. T. Chen, Y. Liu, L. Pan, T. Lu, Y. Yao, Z. Sun, D.H. Chua, and Q. Chen, *J. Mater. Chem. A* 2, 4117 (2014).
36. R. AlcáNtara, G.F. Ortiz, J.L. Tirado, and P. Lavela, *Electrochem. Solid State Lett.* 8, A222 (2005).
37. J. Ding, H. Wang, Z. Li, A. Kohandehghan, K. Cui, Z. Xu, B. Zahiri, X. Tan, E.M. Lotfabad, B.C. Olsen, and D. Mitlin, *ACS Nano* 7, 11004 (2013).
38. E.M. Lotfabad, J. Ding, K. Cui, A. Kohandehghan, W.P. Kalisvaart, M. Hazelton, and D. Mitlin, *ACS Nano* 8, 7115 (2014).
39. N. Sun, H. Liu, and B. Xu, *J. Mater. Chem. A* 3, 20560 (2015).
40. L. Wu, D. Buchholz, C. Vaalma, G.A. Giffin, and S. Passerini, *ChemElectroChem* 27, 231 (2016).
41. W. Luo, J. Schardt, C. Bommier, B. Wang, J. Razink, J. Simonsen, and X. Ji, *J. Mater. Chem. A* 1, 10662 (2013).
42. J. Jin, B.-J. Yu, Z.-Q. Shi, C.-Y. Wang, and C.-B. Chong, *J. Power Sources* 272, 800 (2014).